ESD-TR-84-169

MTR-9055

AD-A142 363

RANGE CORRECTIONS FOR AIRBORNE RADAR — A JOINT STARS STUDY

By
G. A. ROBERTSHAW

MAY 1984

Prepared for
DEPUTY COMMANDER FOR TACTICAL SYSTEMS
ELECTRONIC SYSTEMS DIVISION
AIR FORCE SYSTEMS COMMAND
UNITED STATES AIR FORCE
Hanscom Air Force Base, Massachusetts

DTIC FILE COPY

Project No. 6460
Prepared by
THE MITRE CORPORATION
Bedford, Massachusetts
Contract No. F19628-82-C-0001

UNCLASSIFIED

SECURITY CLASSIFICATION OF THIS PAGE

REPORT DOCUMENTATION PAGE

1a REPORT SECURITY CLASSIFICATION Unclassified	1b RESTRICTIVE MARKINGS
2a SECURITY CLASSIFICATION AUTHORITY	3 DISTRIBUTION/AVAILABILITY OF REPORT Approved for public release; distribution unlimited.
2b DECLASSIFICATION/DOWNGRADING SCHEDULE	
4 PERFORMING ORGANIZATION REPORT NUMBER(S) MTR-9055 ESD-TR-84-169	5. MONITORING ORGANIZATION REPORT NUMBER(S)
6a NAME OF PERFORMING ORGANIZATION The MITRE Corporation 6b. OFFICE SYMBOL (If applicable)	7a NAME OF MONITORING ORGANIZATION
6c. ADDRESS (City, State and ZIP Code) Burlington Road Bedford, MA 01730	7b ADDRESS (City, State and ZIP Code)
8a NAME OF FUNDING/SPONSORING ORGANIZATION Deputy Commander for Tactical Systems 8b OFFICE SYMBOL (If applicable) TCG	9. PROCUREMENT INSTRUMENT IDENTIFICATION NUMBER F19628-82-C-0001
8c ADDRESS (City, State and ZIP Code) Electronic Systems Division Hanscom AFB, MA 01731	10 SOURCE OF FUNDING NOS PROGRAM ELEMENT NO: PROJECT NO.: 6460 TASK NO: WORK UNIT NO:
11. TITLE (Include Security Classification) Range Corrections for Airborne Radar - A Joint STARS Study	
12. PERSONAL AUTHOR(S) G. A. Robertshaw	
13a. TYPE OF REPORT Final Report 13b. TIME COVERED FROM _____ TO _____	14 DATE OF REPORT (Yr., Mo., Day) 1984 May 15 PAGE COUNT 58
16. SUPPLEMENTARY NOTATION	

17 COSATI CODES			18. SUBJECT TERMS (Continue on reverse if necessary and identify by block number)
FIELD	GROUP	SUB GR.	Airborne Radar; Ray Trace; Joint STARS; Refractivity; Range Correction

19. ABSTRACT (Continue on reverse if necessary and identify by block number)

To provide accurate estimates of true target range, all airborne surveillance radars must take into account the effects of the atmospheric medium. The principal contribution to the range correction for atmospheric refractivity arises from the retardation of the propagation speed of the sensing field. Changes in atmospheric density, layer structure, and/or water vapor content, associated with geographical or weather factors, affect the magnitude of the range correction. In the present work, based primarily on USAFETAC ray trace computations performed in support of Joint STARS, range correction variability is examined using atmospheric data collected over three-month periods at Munich and Hannover in Germany, Dhahran in Saudi Arabia, and Pohang in South Korea. Range correction statistics are presented for each location, the predictive value of surface refractivity measurements is assessed, and a simple empirical formula for range correction is developed.

20 DISTRIBUTION/AVAILABILITY OF ABSTRACT UNCLASSIFIED/UNLIMITED ☐ SAME AS RPT ☒ DTIC USERS ☐	21 ABSTRACT SECURITY CLASSIFICATION Unclassified
22a NAME OF RESPONSIBLE INDIVIDUAL Susan R. Gilbert	22b TELEPHONE NUMBER (Include Area Code) (617) 271-8088 22c OFFICE SYMBOL

DD FORM 1473, 83 APR EDITION OF 1 JAN 73 IS OBSOLETE

UNCLASSIFIED

SECURITY CLASSIFICATION OF THIS PAGE

TABLE OF CONTENTS

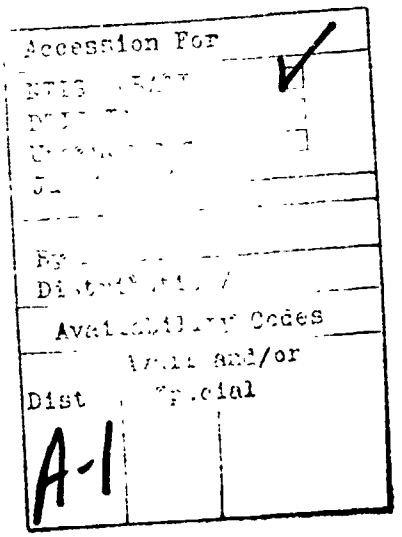

LIST OF ILLUSTRATIONS

LIST OF TABLES

ACKNOWLEDGMENTS

I wish to thank the very competent staff at ETAC, whose members developed the ray trace program and provided the numerical results upon which most of this report is based. I am also indebted to E. W. Beasley and L. P. Shepherd for their guidance and support during the genesis of this paper. And finally, I sincerely appreciate the assistance of Mr. T. Kyle, ESD Staff Meteorologist, who acted as my liaison with ETAC and contributed to this work through many informative discussions with the author.

This document has been prepared by The MITRE Corporation under Project No. 6460, Contract F19628-82-C-0001. The contract is sponsored by the Electronic Systems Division, Air Force Systems Command, Hanscom Air Force Base, Massachusetts.

SECTION 1

INTRODUCTION

In radar, the range of a target can be inferred from the round-trip travel time of an electromagnetic pulse or pulses. While the precision or resolution of a range measurement depends upon the waveform bandwidth, absolute range accuracy must take into account the atmospheric retardation of the propagation speed. For airborne radar, the beam must traverse a layer of atmosphere whose refractive index varies with altitude, geographical location, and local climate and topography. Generally, the correction which must be applied to the indicated radar range, which is obtained from the product of the measured propagation delay and c_0, the speed of light in vacuo, is a function of the detailed "refractivity structure" of the atmosphere throughout the volume which lies over the area of interest.

Ray tracing, which is based upon geometrical optics, provides the theoretical basis for range correction calculations in the context of standard, empirical, or semi-empirical atmospheric models. Basically, ray tracing permits the integration of the effects of refractivity along the path of the radar's beam, and thus yields an estimate of the total excess electromagnetic propagation time for a given source-target geometry.

This report is largely based on refractivity data and associated ray trace computations provided by the U.S. Air Force Environmental Technical Applications Center (ETAC) at Scott AFB, IL, in support of the Joint STARS program. These computations and subsequent work were undertaken to determine good estimates for radar range corrections under a variety of geographical, climatic, and geometrical circumstances. The effect of atmospheric variability on the range correction is of particular interest, since potential performance specifications are ultimately limited by uncontrollable and/or unknown weather factors.

The essential methods, assumptions, and results of these studies are covered in the following sections. In section 2 the basic method employed to model the atmosphere is discussed, while section 3 provides a tutorial review of the underlying definitions and concepts of range correction. Although well-informed readers may wish to skip section 3, the definitions at the beginning of the section should be reviewed by all readers to avoid possible subsequent confusion. In section 4, the results of range correction calculations in the context of a standard atmosphere model are presented. Section 5 contains a

description and analysis of the ETAC ray trace results, and provides many tables for quick reference. The topic of range correction in the context of a standard atmosphere is reconsidered in section 6, which provides an empirical formula for range correction as a function of radar range, surface refractivity, and radar altitude. Conclusions are summarized in section 7.

Histograms which conveniently illustrate details of the ETAC range correction results are provided in appendix A, while short climactic descriptions for the geographical regions near or at the radiosonde data collection sites are given in appendix B.

SECTION 2

METHOD

To estimate the effect of the atmosphere on radar wave (e.g., X-band) propagation at a given geographical location, local measurements of the atmosphere's vertical refractivity profile are required. An estimate of the true profile can be deduced from routine radiosonde data obtained over the area of interest. Ideally, a full three-dimensional sampling volume should be employed to characterize the local propagation environment, however, under most circumstances such detailed data collection is impractical. If only a single vertical profile exists for a given time and place, lateral homogeneity is usually assumed. ETAC has also adopted this "stratified atmosphere" model for the local propagation environment. Clearly, as the area of interest is expanded, the model's validity weakens, since the atmosphere is dynamic and inhomogeneous over larger areas. Nevertheless, the assumption of stratification represents the simplest and most fruitful use of radiosonde data acquired during a single ascent.

While horizontal variation is entirely neglected, poor vertical resolution may also contribute to the atmospheric model's inaccuracies. Radiosonde temperature and humidity data is reported at altitudes which suit the purposes of the meteorologist and reflect the limited response times of the various instruments. Therefore, relatively thin atmospheric layers with high refractivity gradients are likely to be missed or "smeared out" in the vertical radiosonde profile representation. For very low grazing angles, as occur near the radar horizon, such inaccuracies can lead to erroneous ray trace predictions. However, in view of the Joint STARS sample geometries discussed in section 5, the radiosonde derived refractivity profiles are deemed adequate.

Ray trace calculations are performed within this semi-empirical atmosphere model. The ray trace algorithm developed at ETAC principally provides estimates of range correction and path bending in the context of specified geometrical constraints.

SECTION 3

BASIC THEORY AND DEFINITIONS

In discussions involving the radar range to a target, care must be exercised in specifying exactly what is meant by "range" if the propagation path lies in or crosses the atmosphere. At least three "types" of range can immediately be defined:

1. R_s: The geometric, straight line separation between the target and the radar (also called "true range").

2. R_p: The geometric separation of the target and radar, as measured along the propagation path of the electromagnetic waves emitted by the radar.

3. R_t: the radar range, i.e., the range given by the product of one half the round trip travel time of a pulse reflected by a target and the speed of light in vacuo, c_o.

If the propagation path lies completely in free space:

$$R_s = R_p = R_t$$

However, for propagation in an inhomogeneous medium, such as the atmosphere (on the scale of surveillance radar ranges):

$$R_t > R_p > R_s$$

If very accurate target location information is required, R_s, the true geometric slant range, must be determined. On the other hand, the round trip to target pulse travel time, and hence R_t, is the physical quantity measured by the radar. For many applications, the difference between R_s and R_t is entirely insignificant. However, in view of the stringent accuracies specified for modern surveillance and targeting radars, the range errors incurred by using R_t instead of R_s may not be tolerable.

Consider the greatly simplified propagation environment illustrated in figure 1. The medium consists of two adjacent homogeneous layers of atmosphere. The source, with coordinates $(0, h_1 + h_2)$

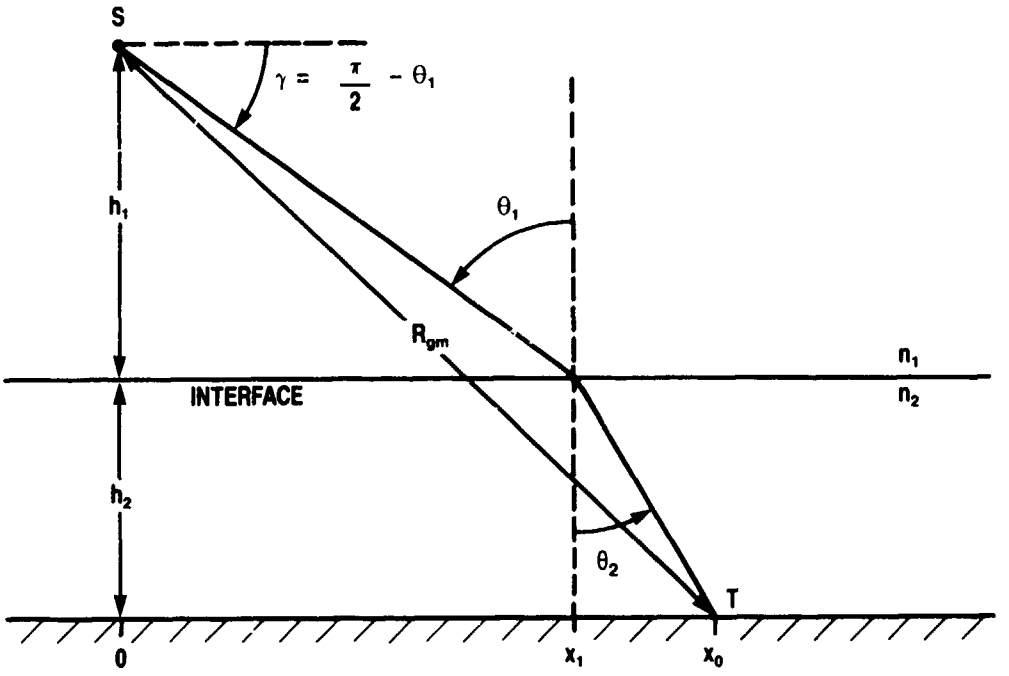

Figure 1. Simplified Propagation Environment

lies in the upper layer, which has a refractive index n_1, while the target, with coordinates $(x_0, 0)$, lies on the surface in the lower layer, which has a refractive index n_2. The layer interface lies at an altitude h_2. Under these circumstances, the paths of electromagnetic waves can be represented by rays, and within each layer the rays are straight since the media are homogeneous. The bending of the path at the layer interface can be understood as a consequence of the different propagation speeds of the waves in the two regions. The propagation speeds are related to the respective refractive indices by:

$$c_1 = \frac{c_o}{n_1} \; ; \qquad c_2 = \frac{c_o}{n_2} \tag{3,4}$$

in which c_0 is the speed of light in vacuo. The total time required for propagation from the source to the target may therefore be expressed:

$$\Delta t = \frac{(h_1^2 + x_1^2)^{\frac{1}{2}}}{c_1} + \frac{(h_2^2 + (x_o - x_1)^2)^{\frac{1}{2}}}{c_2} \tag{5}$$

in which x_1, the x-coordinate of ray intersection at the interface, remains to be determined. To fix x_1 it is sufficient, in principle, to recognize that electromagnetic waves traverse that path which minimizes the total travel time between two points. This concept, known as Fermat's principle, obviously holds for straight line propagation in homogeneous media and specular reflection, for which the angle of incidence is equal to the angle of reflection. Thus, the value of x_1 which minimizes Δt characterizes the intersection of the ray at the interface in figure 1. To find the minimum Δt, equation (5) is differentiated with respect to x_1 and the derivative is set equal to zero:

$$\frac{d(\Delta t)}{dx_1} = \frac{x_1}{c_1(h_1^2 + x_1^2)^{\frac{1}{2}}} + \frac{x_o - x_1}{c_2(h_2^2 + (x_o - x_1)^2)^{\frac{1}{2}}} = 0 \tag{6}$$

If use is made of the angles θ_1, and θ_2, as defined in figure 1, equation (6) may be expressed:

$$n_1 \sin\theta_1 - n_2 \sin\theta_2 = 0 \tag{7}$$

which is just the familiar Snell's law of refraction. Rather than proceed to solve equation (6) for x_1 and substitute the result into equation (5) to obtain Δt for the path from S to T, it is simpler to specify the source height $(h_1 + h_2)$ and the ray launch angle γ $(\gamma = \pi/2 - \theta_1)$, and trace the ray's path to a target position, which is now a dependent variable. The three ranges defined at the beginning of this section are then given by:

$$R_s = \left[(h_1 + h_2)^2 + (h_1 \tan\theta_1 + h_2 \tan\theta_2)^2 \right]^{\frac{1}{2}} \tag{8}$$

$$R_p = \frac{h_1}{\cos\theta_1} + \frac{h_2}{\cos\theta_2} \tag{9}$$

$$R_t = \frac{n_1 h_1}{\cos\theta_1} \quad \frac{n_2 h_2}{\cos\theta_2} \tag{10}$$

in which

$$\theta_1 = \frac{\pi}{2} - \gamma \tag{11}$$

and

$$\theta_2 = \sin^{-1}\left[\frac{n_1 \sin\theta_1}{n_2}\right] \tag{12}$$

For illustration, consider the following numerical example based on the simple two layer propagation environment of figure 1. The ray trace input variables and constants are:

h_1 = 10 kft. = 3.048 km

h_2 = 5 kft. = 1.524 km

γ = 1.5°

n_1 = 1.000150 (refractivity = 150 N-units)

n_2 = 1.000300 (refractivity = 300 N-units)

and by use of equations (8) through (12):

$\theta_1 = 88.5°$

$\theta_2 = 88.20157°$ km

$R_s = 164.99864$ km

$R_p = 164.99911$ km

$R_t = 165.03114$ km

As the results above show, R_s and R_p are practically equal:

$$R_p - R_s \cong 0.47 \text{ m}$$

The difference between R_t and R_s is also small but not necessarily insignificant:

$$R_t - R_s \cong 32.5 \text{ m}$$

For the present purpose, the range correction is defined:

$$R_c = R_t - R_s \cong R_t - R_p \tag{13}$$

Thus, true range may be obtained from the radar measured range by subtraction of a range correction. The range correction may be considered a function of R_t for convenience, and the actual numerical dependence can be estimated by ray tracing. In the simple example discussed above, a range correction of 32.5 m at 165 km radar range (R_t) was noted. For $R_t = 85.9$ km ($\gamma = 3°$), however, a similar calculation shows that the range correction is only 17 m. This is a sensible result, since the range correction should be approximately proportional to R_t, for given source and target altitudes.

The influence of the vertical refractivity profile on the range correction is considered in detail in the following sections.

SECTION 4

RANGE CORRECTIONS IN THE CONTEXT OF A STANDARD ATMOSPHERIC MODEL

The propagation environment illustrated in figure 1 is certainly not a good representation of the earth's atmosphere, however, the underlying modeling concept is a fruitful one. The stratified, spherically symmetric model atmosphere, in which propagation is rectilinear within shells and refraction occurs at shell boundaries, has been described in detail elsewhere.[1] If the rays, which represent the path of electromagnetic energy, pass through a total of M shells, the range, as measured along the propagation path, is, to a good approximation:

$$R_p \cong \sum_{m=1}^{M} r_m \tag{14}$$

in which the r_m's are the intrashell ray segment lengths. If the refractive index of shell "m" is denoted by n_m, the corresponding radar range is:

$$R_t \cong \sum_{m=1}^{M} r_m n_m \tag{15}$$

In view of the above expression, changes in the model atmospheric refractivity profile can be expected to have a significant impact on the range correction. Since R_p is, for practical purposes, equal to R_s:

$$R_c \cong \sum_{m=1}^{M} (n_m - 1) r_m = 10^{-6} \sum_{m=1}^{M} N_m r_m \tag{16}$$

in which N_m is the refractivity in the mth shell.

The results described in this section are calculated in the context of a standard refractivity profile which represents an average of conditions worldwide.[2] Input parameters for the model profile are the refractivity at the surface (N_s) and the surface height with respect to mean sea level (MSL).

Ray trace calculations in which the atmosphere between the source and target is divided into 100 concentric shells have been performed for three refractivity profiles at each of three source (radar) altitudes. The surface elevation for all of these cases was 1 kft. MSL, and the three profiles were obtained by setting N_s equal to 200, 300, and 400 N-units, respectively.

Plots of range correction* versus radar range, as derived from the ray trace computations, are presented in figures 2, 3, and 4, for hypothetical radar altitudes (MSL) of 15, 35, and 65 kft., respectively. The following general comments apply:

1. At each radar altitude, the range correction increases with increasing surface refractivity, N_s.

2. The range correction is a nearly linear function of radar range.

3. Relative variation in the range correction due to changes in N_s becomes progressively less pronounced as the radar altitude is increased.

All of the above results are sensible, and could have been predicted on the basis of the simple two layer model of figure 1. The much more elaborate ray trace computations, however, permit accurate estimates of the size of the correction factor under particular circumstances of interest. A typical curve of range correction versus radar range is produced by a manual fit to up to 30 discrete, ray trace derived, points. Since the curves are nearly linear from their lower limits to 200 km, a linear regression fit was performed for each one, using all points with abscissas less than 200 km. The range correction is then, to a good approximation:

$$R_c \cong a + b\, R_t \tag{17}$$

in which R_c has units of meters and R_t has units of kilometers. The fit parameters, a and b, are given in table 1 for the nine cases. Although the linear form was chosen for simplicity, a more general polynomial fit would undoubtedly produce better correlation with the ray trace points over the entire range.

*Strict definition, $R_c = R_t - R_s$, is used.

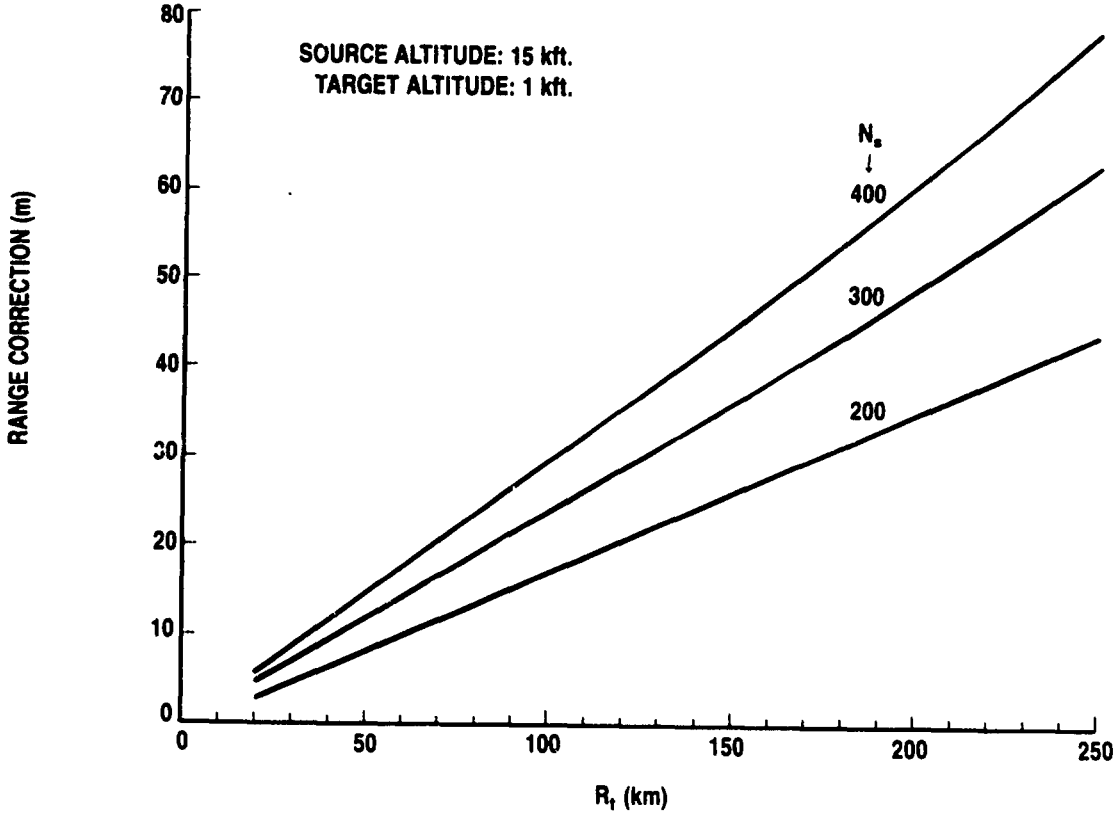

Figure 2. Range Correction Versus Radar Range - 15 kft. (MSL)

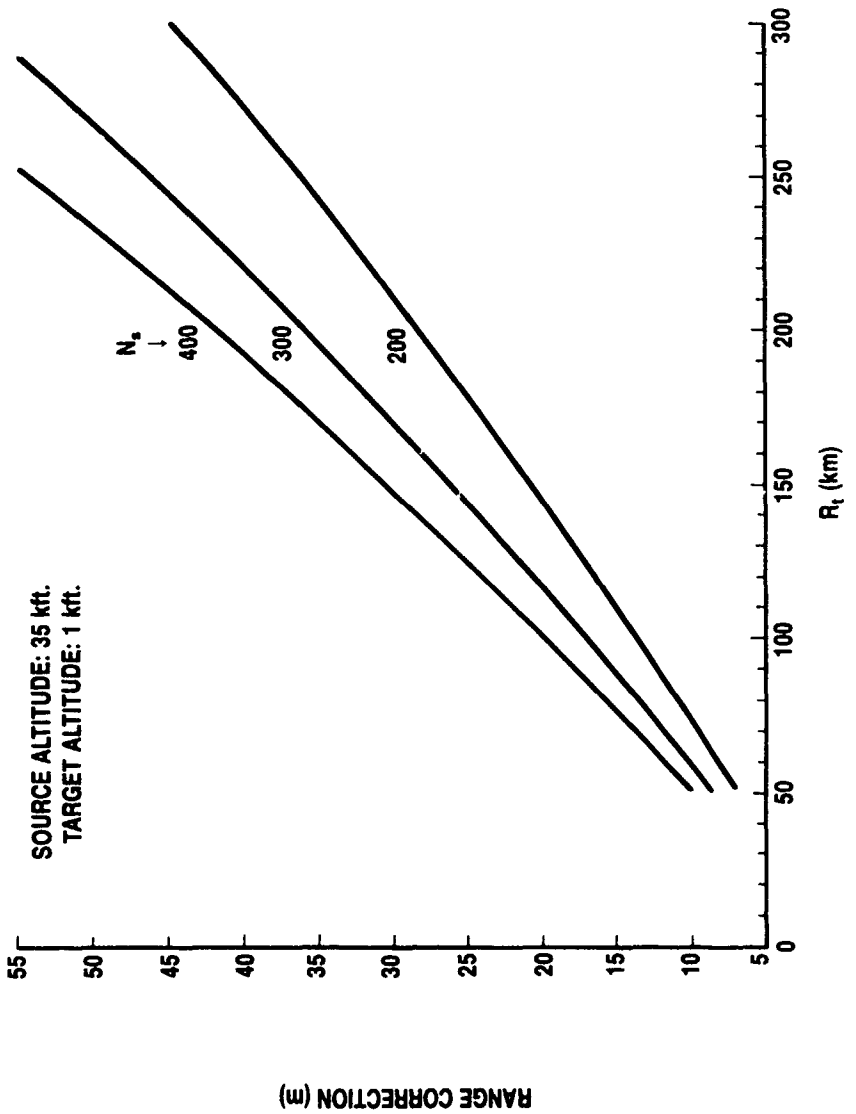

Figure 3. Range Correction Versus Radar Range - 35 kft. (MSL)

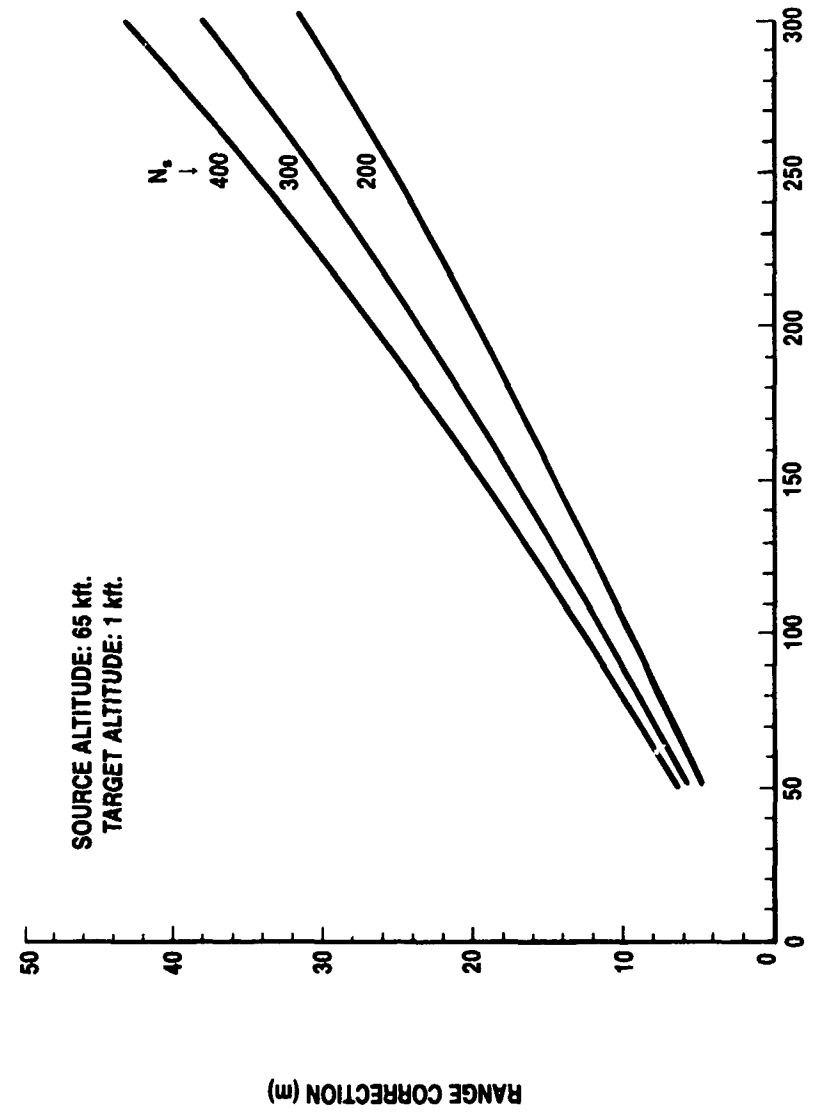

Figure 4. Range Correction Versus Radar Range - 65 kft. (MSL)

Table 1

Linear Regression Parameters for Range Correction

RADAR ALTITUDE (kft)	SURFACE REFRACTIVITY (N-units)	INTERCEPT a (m)	SLOPE b (m/km)
15	200	-0.38	0.173
15	300	-0.59	0.244
15	400	-0.89	0.305
35	200	-0.32	0.141
35	300	-0.62	0.179
35	400	-0.86	0.211
65	200	-0.30	0.099
65	300	-0.43	0.119
65	400	-0.59	0.135

For the standard atmospheric model, range correction is a function of three independent variables: 1) Radar altitude (h) with respect to mean sea level (MSL), 2) Surface refractivity (N_s), and 3) Radar indicated range, R_t.

$$R_c = F(h, N_s, R_t) \tag{18}$$

Strictly speaking, terrain elevation should be included as a fourth variable, however, a nominal surface height of 1000 feet may be assumed for simplicity. A series of ray traces, which span the variable ranges of interest, may be performed, as was done to produce figures 2, 3, and 4. Multiple polynomial regression may then be used to determine a suitable range correction function (equation 18), or

alternatively, the ray trace results may be incorporated in a lookup table, with linear interpolation used to obtain intermediate values. A simple empirical range correction function is developed in section 6.

The value of the procedures outlined above hinges, of course, on the applicability of the standard atmosphere model. Actual refractivity profiles often exhibit superrefractive and subrefractive layers within which the refractivity gradient assumes abnormally low or high values, respectively. Under certain conditions such layers may trap or otherwise deflect radar waves, and the standard range correction may be rendered grossly inaccurate. In the next section, the ETAC data and ray trace results are examined in order to provide a far more realistic framework in which to assess the feasibility and accuracy of range correction in typical Joint STARS propagation environments.

SECTION 5

DESCRIPTION AND ANALYSIS OF ETAC RAY TRACE RESULTS

The ray trace computations discussed in this section are predicated upon atmospheric data collected at sites in Hannover and Munich in Germany, Dhahran in Saudi Arabia, and Pohang in South Korea. The precise locations and elevations of the sites are given in table 2. Three months of data spanning up to three years (e.g., May, June, and July of 1979, 1980, and 1981 for Pohang) were selected for each site on the basis of their larger than average refractivity gradient variability for the region within 100 m of ground level. On each day of a given month, with occasional but sometimes frequent (e.g., Pohang) omissions, refractivity profiles based on radiosonde data collected at 0:00 GMT and 12:00 GMT were provided. Thus, for a typical two month data set, about 55 profiles were available for each time.

Each refractivity profile was used by ETAC to define a model stratified atmosphere, in which refractivity is a function of altitude only. Ray trace computations were performed for three sensor-target geometries which are characterized as follows:

1. Low: The radar is positioned at an altitude of 15 kft. (4.57 km) above mean sea level (MSL), with the target at a nominal ground range of 222 km.

2. Medium: The radar is positioned at an altitude of 35 kft. (10.67 km) MSL, with the target at a nominal ground range of 279 km.

3. High: The radar is positioned at an altitude of 65 kft. (19.81 km), with the target at a nominal ground range of 279 km.

The range correction, as defined in section 3, represents the difference between the radar range and geometric range (equation 13). As shown earlier, the main contribution to the range correction arises from the reduced speed of radar waves in the atmospheric medium, with respect to free space propagation.

Summary tables 3, 4, 5 and 6 contain range correction statistics based on the ETAC ray traces for profiles corresponding to the Munich, Hannover, Dhahran, and Pohang sites, respectively. The mean and standard deviation of each set of range correction values pertaining to a given month and time are provided. In addition, the upper and

Table 2

Sites of Radiosonde Data Collection for
ETAC Ray Trace Computations

SITE	LATITUDE	LONGITUDE	ELEVATION
Munich, Germany	48.2500 N	11.6001 E	1,588 ft. (484 m)
Hannover, Germany	52.4700 N	9.7202 E	180 ft. (55 m)
Dhahran, Saudi Arabia	26.2698 N	50.1802 E	75 ft. (23 m)
Pohang, South Korea	36.0298 N	129.4001 E	16 ft. (5 m)

Table 3

Statistical Summary for Munich Ray Traces

GEOMETRY	MEASUREMENT PERIODS	TIME (GMT)	RANGE CORRECTION STATISTICS			
			AVERAGE (m)	STANDARD DEVIATION (m)	BOUNDS (m)	NO. OF RUNS
Low	Jun. 79, 80	12	57.8	1.29	54.7, 60.1	58
	Jun. 79, 80	0	58.1	1.18	56.2, 61.8	54
	Aug. 78, 80	12	58.0	1.75	53.3, 60.9	56
	Aug. 78, 80	0	57.9	1.56	54.9, 61.8	58
	Sep. 79, 80	12	57.4	1.36	54.0, 60.4	55
	Sep. 79, 80	0	57.5	1.45	54.0, 60.5	55
Medium	Jun. 79, 80	12	54.2	0.81	52.2, 55.9	58
	Jun. 79, 80	0	54.4	0.82	53.0, 56.9	58
	Aug. 78, 80	12	54.2	1.19	50.8, 56.4	56
	Aug. 78, 80	0	54.2	1.08	52.0, 56.4	58
	Sep. 79, 80	12	53.8	1.06	51.5, 56.2	58
	Sep. 79, 80	0	53.8	1.08	51.8, 56.4	56
High	Jun. 79, 80	12	35.6	0.51	34.7, 36.6	58
	Jun. 79, 80	0	35.7	0.55	34.7, 37.4	58
	Aug. 78, 80	12	35.6	0.63	33.9, 36.6	56
	Aug. 78, 80	0	35.6	0.61	34.4, 36.6	58
	Sep. 79, 80	12	35.5	0.53	34.4, 36.6	58
	Sep. 79, 80	0	35.5	0.56	34.7, 37.1	56

Table 4

Statistical Summary for Hannover Ray Traces

GEOMETRY	MEASUREMENT PERIODS	TIME (GMT)	RANGE CORRECTION STATISTICS			
			AVERAGE (m)	STANDARD DEVIATION (m)	BOUNDS (m)	NO. OF RUNS
Low	Jun. 78, 80	12	58.9	1.61	55.1, 62.9	50
	Jun. 78, 80	0	58.9	1.62	54.9, 62.1	46
	Jul. 78, 80	12	59.3	1.30	57.1, 63.2	54
	Jul. 78, 80	0	59.2	1.39	56.4, 63.7	51
	Aug. 79, 80	12	59.5	1.50	57.0, 62.8	53
	Aug. 79, 80	0	59.6	1.44	57.1, 62.7	56
Medium	Jun. 78, 80	12	55.4	1.15	52.7, 58.3	50
	Jun. 78, 80	0	55.4	1.23	52.2, 57.9	46
	Jul. 78, 80	12	55.6	0.88	53.7, 58.1	54
	Jul. 78, 80	0	55.6	1.04	53.5, 58.6	51
	Aug. 79, 80	12	55.8	1.11	53.7, 58.1	53
	Aug. 79, 80	0	55.9	1.08	54.0, 58.3	56
High	Jun. 78, 80	12	36.5	0.71	35.2, 38.1	50
	Jun. 78, 80	0	36.5	0.74	34.9, 37.8	46
	Jul. 78, 80	12	36.6	0.50	35.6, 38.3	54
	Jul. 78, 80	0	36.5	0.62	35.6, 38.3	51
	Aug. 79, 80	12	36.7	0.70	35.4, 38.1	53
	Aug. 79, 80	0	36.8	0.67	35.6, 38.3	56

Table 5

Statistical Summary for Dhahran Ray Traces

GEOMETRY	MEASUREMENT PERIODS	TIME (GMT)	RANGE CORRECTION STATISTICS			
			AVERAGE (m)	STANDARD DEVIATION (m)	BOUNDS (m)	NO. OF RUNS
Low	May 78, 79, 80	12	53.7	1.69	50.8, 59.6	59
	May 78, 79, 80	0	54.6	1.87	51.2, 59.6	60
	Jun 78, 79, 80	12	52.9	2.61	49.9, 62.1	56
	Jun 78, 79, 80	0	53.1	1.80	50.5, 60.2	50
	Oct 79, 80	12	55.6	1.94	51.3, 60.5	47
	Oct 79, 80	0	56.3	2.06	52.4, 63.4	62
Medium	May 78, 79, 80	12	52.3	1.28	50.0, 56.6	59
	May 78, 79, 80	0	52.5	1.20	50.3, 56.2	61
	Jun 78, 79, 80	12	51.2	1.98	48.8, 57.9	54
	Jun 78, 79, 80	0	51.4	1.78	49.6, 59.8	54
	Oct 79, 80	12	53.1	1.26	50.0, 55.9	47
	Oct 79, 80	0	53.4	1.58	50.8, 60.1	64
High	May 78, 79, 80	12	35.4	0.64	34.4, 37.6	59
	May 78, 79, 80	0	35.5	0.65	34.4, 37.4	61
	Jun 78, 79, 80	12	35.0	1.09	33.7, 38.3	53
	Jun 78, 79, 80	0	35.0	0.98	33.7, 39.6	54
	Oct 79, 80	12	35.7	0.63	34.2, 37.1	47
	Oct 79, 80	0	35.9	0.94	34.7, 41.0	64

Table 6

Statistical Summary for Pohang Ray Traces

GEOMETRY	MEASUREMENT PERIODS	TIME (GMT)	RANGE CORRECTION STATISTICS			
			AVERAGE (m)	STANDARD DEVIATION (m)	BOUNDS (m)	NO. OF RUNS
Low	May 79, 80, 81	12	57.5	2.55	53.6, 61.0	17
	May 79, 80, 81	0	57.9	2.93	54.5, 64.5	15
	Jun 79, 80, 81	12	60.8	2.27	55.6, 65.5	35
	Jun 79, 80, 81	0	60.9	2.98	52.7, 65.1	34
	Jul 79, 80, 81	12	63.6	2.10	59.6, 67.0	23
	Jul 79, 80, 81	0	63.2	2.37	58.3, 67.2	31
Medium	May 79, 80, 81	12	54.6	1.77	51.8, 57.4	17
	May 79, 80, 81	0	55.0	2.02	53.0, 60.1	15
	Jun 79, 80, 81	12	56.8	1.72	53.2, 60.5	35
	Jun 79, 80, 81	0	56.9	2.16	51.5, 60.3	35
	Jul 79, 80, 81	12	58.7	1.87	55.4, 61.8	24
	Jul 79, 80, 81	0	58.5	1.89	54.9, 61.8	32
High	May 79, 80, 81	12	36.4	0.96	34.9, 37.8	17
	May 79, 80, 81	0	36.5	1.11	35.4, 39.3	15
	Jun 79, 80, 81	12	37.7	1.03	35.9, 40.0	35
	Jun 79, 80, 81	0	37.7	1.14	34.9, 39.6	35
	Jul 79, 80, 81	12	38.7	1.06	36.9, 40.5	24
	Jul 79, 80, 81	0	38.6	1.11	36.6, 40.5	32

lower bounding range correction values and total number of values in each month-time group are given. The following general observations deserve emphasis:

1. The standard deviation of the range correction is always a small fraction of the corresponding mean value for any given month.

2. The standard deviation of the range correction, as a percentage of the mean value (coefficient of variation) decreases with increasing sensor altitude.

3. For a given site and sensor-target geometry (low, medium, or high) the mean and standard deviation of the range correction do not show large or systematic variations with time of day and month.*

4. Mean range corrections are relatively low for Dhahran and relatively high for Pohang, while the German sites yield intermediate values.

The second of the above points is quite reasonable since, for a given ground range, a lower altitude sensor incurs a propagation path which crosses more of the lower, more variable atmosphere than the path incurred by a higher altitude sensor. The lower altitude sensor's ray path also suffers lower grazing angles (relative to atmospheric strata) which may contribute to anomalous propagation effects at or near ranges which correspond to the lower sensor's radio horizon.

The Saudi Arabian and Korean sites display much greater intermonth variation of range correction means than the German sites. In the most general sense, this observation can be understood as a consequence of the more extreme atmospheric variability which characterizes Dhahran and Pohang.**

*Small monthly variations are evident for Dhahran and Pohang, as illustrated in appendix A, however, more data would be required to determine if these variations are statistically significant.

**General climactic descriptions for the sites are provided in appendix B.

Table 7 presents a statistical overview of the ETAC ray trace results and surface refractivities, which are taken from the corresponding profiles. For each site the overall mean and standard deviation of both the range correction and surface refractivity* are provided, for each propagation geometry. In addition, combined statistics, which include all the site results taken together, appear at the bottom of the table. Surface refractivity was selected for further study in the context of the ray trace work, since this quantity is easily measured and its statistics are available for various locations throughout the world.[3] As examination of the table reveals, the Korean and Saudi sites have larger range correction variations than the German sites. At first, the noted variability of the range correction appears to be loosely associated with variability of the surface refractivity, since there appears to be some correlation between the range correction and surface refractivity standard deviations. The relationship between range correction and surface refractivity will be examined in some detail towards the end of this section.

The combined statistics for the four sites clearly support points 1 and 2 above. Even the bounding values do not deviate far enough from the respective mean values to cause alarm, in the context of the Joint STARS accuracy objectives.

Although the ETAC ray traces were limited to three basic geometries, the cases chosen are sufficiently stressful to permit a comparison against the standard refractivity model, which provided the basis for the range corrections of figures 2, 3, and 4. In table 8, the mean range corrections of table 7 are compared with MITRE ray trace predictions based on a standard atmosphere characterized by the mean surface refractivity and elevation at the given site. The agreement obtained is excellent, with the exception of the Dhahran examples. These results show that for three out of the four sites considered, good estimates of the mean range correction values are obtained by ray traces performed in the context of the standard refractivity profile based on the mean surface refractivity and elevation of the site.

*Ideally, surface refractivity statistics are geometry independent, as is the case for Hannover in table 7. Small differences appear for the other sites since certain combinations of radar geometry and refractivity profile produced erroneous ray traces which had to be omitted from table 7. ETAC has since devised program modifications which either correct or suppress the erroneous results.

Table 7

Statistical Overview

SITE (ELEV.)	RADAR GEOMETRY	RANGE CORRECTION STATISTICS (m)			SURFACE REFRACTIVITY STATS (N-UNITS)		NUMBER OF RUNS
		MEAN	STANDARD DEVIATION	BOUNDING VALUES	MEAN	STANDARD DEVIATION	
MUNICH, GERMANY (1,588 ft.)	LOW	57.8	1.46	53.3, 61.8	317.2	9.8	336
	MEDIUM	54.1	1.04	50.8, 56.9	316.8	9.9	344
	HIGH	35.6	0.57	33.9, 37.4	316.8	9.9	344
HANNOVER, GERMANY (180 ft.)	LOW	59.2	1.50	54.9, 63.7	330.7	11.0	310
	MEDIUM	55.6	1.10	52.2, 58.6	330.7	11.0	310
	HIGH	36.6	0.67	34.9, 38.3	330.7	11.0	310
DHAHRAN, SAUDI ARABIA (75 ft.)	LOW	54.4	2.37	49.9, 63.4	327.5	30.1	334
	MEDIUM	52.3	1.73	48.8, 60.1	327.2	30.3	339
	HIGH	35.4	0.90	33.7, 41.0	327.3	30.3	338
POHANG, SOUTH KOREA (16 ft.)	LOW	61.1	3.25	52.7, 67.2	350.4	17.4	155
	MEDIUM	57.0	2.36	51.5, 61.8	350.3	17.5	158
	HIGH	37.8	1.34	34.9, 40.5	350.3	17.5	158
COMBINED	LOW	57.6	3.12	49.9, 67.2	328.4	21.8	1,135
	MEDIUM	54.4	2.22	48.8, 61.8	328.2	21.9	1,151
	HIGH	36.1	1.18	33.7, 41.0	328.3	21.9	1,150

Table 8

Comparison of ETAC Results and Standard Model

SITE	RADAR GEOMETRY	GROUND RANGE (km)	MEAN ETAC RANGE CORRECTION (m)	MITRE STANDARD RANGE (m) CORRECTION	ETAC RANGE CORRECTION STANDARD DEVIATION (m)	MITRE STANDARD RANGE CORR. STANDARD DEVIATION (m)
MUNICH	LOW	222.39	57.8	58.5	1.46	1.49
	MEDIUM	277.99	54.1	54.6	1.04	1.05
	HIGH	277.99	35.6	35.7	0.57	0.52
HANNOVER	LOW	222.55	59.2	59.3	1.50	1.58
	MEDIUM	278.19	55.6	55.9	1.10	1.12
	HIGH	278.19	36.6	36.8	0.67	0.59
DHAHRAN	LOW	221.58	54.4	58.5	2.37	4.22
	MEDIUM	276.98	52.3	55.2	1.73	3.01
	HIGH	276.98	35.4	36.4	0.90	1.57
POHANG	LOW	221.92	61.1	61.1	3.25	3.07
	MEDIUM	277.40	57.0	56.9	2.36	2.36
	HIGH	277.40	37.8	37.4	1.34	1.14

Standard atmosphere model based estimates of the range correction standard deviation can be obtained by performing a ray trace in a standard atmosphere with a surface refractivity given by the sum of the mean surface refractivity and its standard deviation. The difference between the range correction thus obtained and the range correction associated with the mean surface refractivity is generally close in value to the ETAC ray trace results, as inspection of table 8 reveals. The Saudi case is anomalous, since the large variations of surface refractivity which are measured imply a larger range correction variation than is computed by ETAC.

The relatively poor agreement seen in table 8 for the Dhahran range correction statistics deserves further scrutiny. The mean surface refractivity of about 327 N-units, when used to define a standard atmosphere, leads to standard range corrections which are too large in comparison to the ETAC mean range corrections. This discrepancy, which is not seen for the other sites, may be linked to unusual atmospheric conditions which often occur in this part of the world. More specifically, it is not uncommon for hot dry desert air to lie above a relatively narrow, cooler, moister layer of Persian Gulf air at the surface.* Since the surface layer, which is cool and moist, has a much higher refractivity than the hot, dry air above, a pronounced superrefractive or trapping layer is often formed near the surface, as characterized by a steep negative refractivity gradient. The refractivity profile of figure 5, for 0:00 GMT October 5, 1980, exemplifies the condition discussed above. A large surface refractivity of 400.88 N-units is associated with a superrefractive layer which extends to a height no greater than 0.55 km above the surface. The average gradient of this layer is no less than -23 N-units per 100 m. For a standard atmosphere referenced to 400.88 N-units at the surface, a range correction of 68.4 m is obtained via the MITRE ray trace -- greatly in excess of the 55.94 m ETAC result reported for the actual profile. As shown in the figure, a standard profile corresponding to a surface refractivity of 300 N-units has a better overall fit to the measured profile, and the associated range correction of 54.5 m is in far better agreement with the ETAC value. Clearly, the frequent occurrence of such superrefractive layers near the surface biases the surface refractivity-derived, standard atmosphere range corrections towards higher values than those obtained by use of the actual profiles. While subrefractive layers do occasionally occur also, their frequency is insufficient to offset the bias introduced by a larger number of superrefractive surface layers.

*See appendix B.

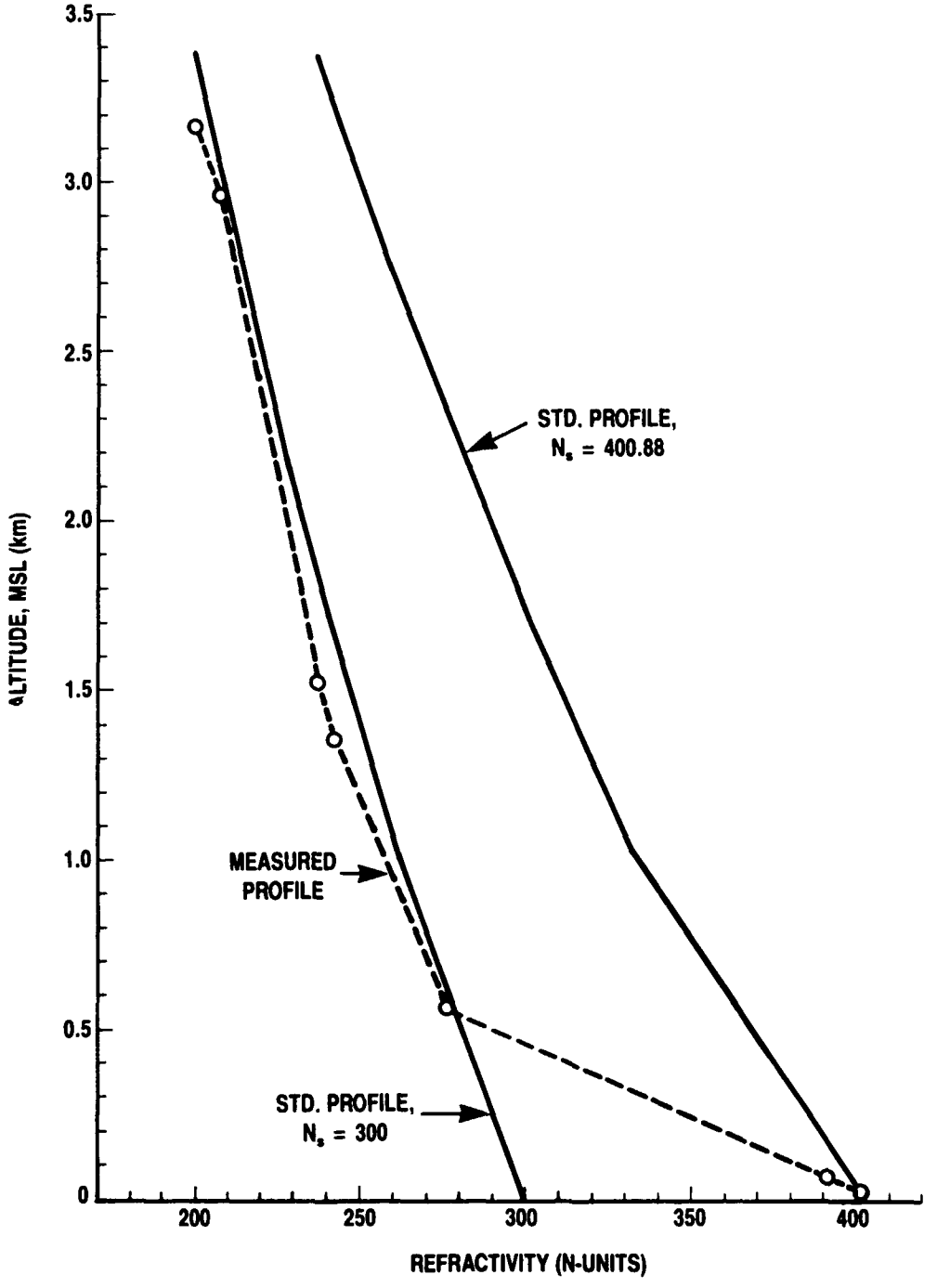

Figure 5. Comparison of October 5, 1980, 00:0 GMT Profile at Dhahran and Standard Profiles

The close agreement between the range corrections derived from ray tracing using standard and measured profiles is encouraging. For three out of four of the sites considered, the mean range correction could have been predicted with very good accuracy by performing a ray trace in the context of the standard atmospheric profile as characterized by the site's mean surface refractivity and elevation. Even in the case of Dhahran, the discrepancy of up to 4.1 m is not serious in view of Joint STARS accuracy requirements. For the propagation geometries considered, the variations in the detailed layering of the atmosphere do not appear to introduce large variations in the range correction. Consider the measured profile of figure 6, for Dhahran on June 5, 1978 at 12:00 GMT. Altogether, this profile exhibits three superrefractive layers and one subrefractive layer as indicated. A standard atmospheric profile, with a surface refractivity of 275 N-units, was fitted by eye to the ill-behaved profile. Low geometry ray traces gave range corrections of 51.56 and 50.65 m for the measured and standard profiles respectively, while for medium geometry ray traces, range corrections of 50.29 and 49.53 m were obtained for the measured and standard profiles, respectively. Although the standard profile completely neglects the deviant N-structure of the measured profile, the computed range correction is only slightly perturbed.

A relationship between surface refractivity and range correction would be especially useful, since surface refractivity is relatively easy to measure in the field. For standard refractivity profiles, range correction increases monotonically with surface refractivity, since the profiles characterized by higher surface refractivities have refractivities at all altitudes which are greater than or equal to the values for profiles having lower surface refractivities. On the other hand, for real atmospheric profiles, surface refractivity is highly variable and is not a reliable indicator of refractivities aloft. To explore the relationship between the range correction and surface refractivity, results for several months, typically those with the highest range correction standard deviations, were selected for further examination.

In figure 7, surface refractivity is plotted against range correction for 56 profiles obtained during August of 1978 and 1980 at Munich, 12:00 GMT. Although there is a definite tendency for larger range corrections to correspond to higher values of surface refractivity, the correlation is visually undramatic. A linear regression line derived from the plotted points is also shown in figure 7. A rough estimate of the range correction is given by:

$$R_C = 0.215\ [N_S - 45.04]$$

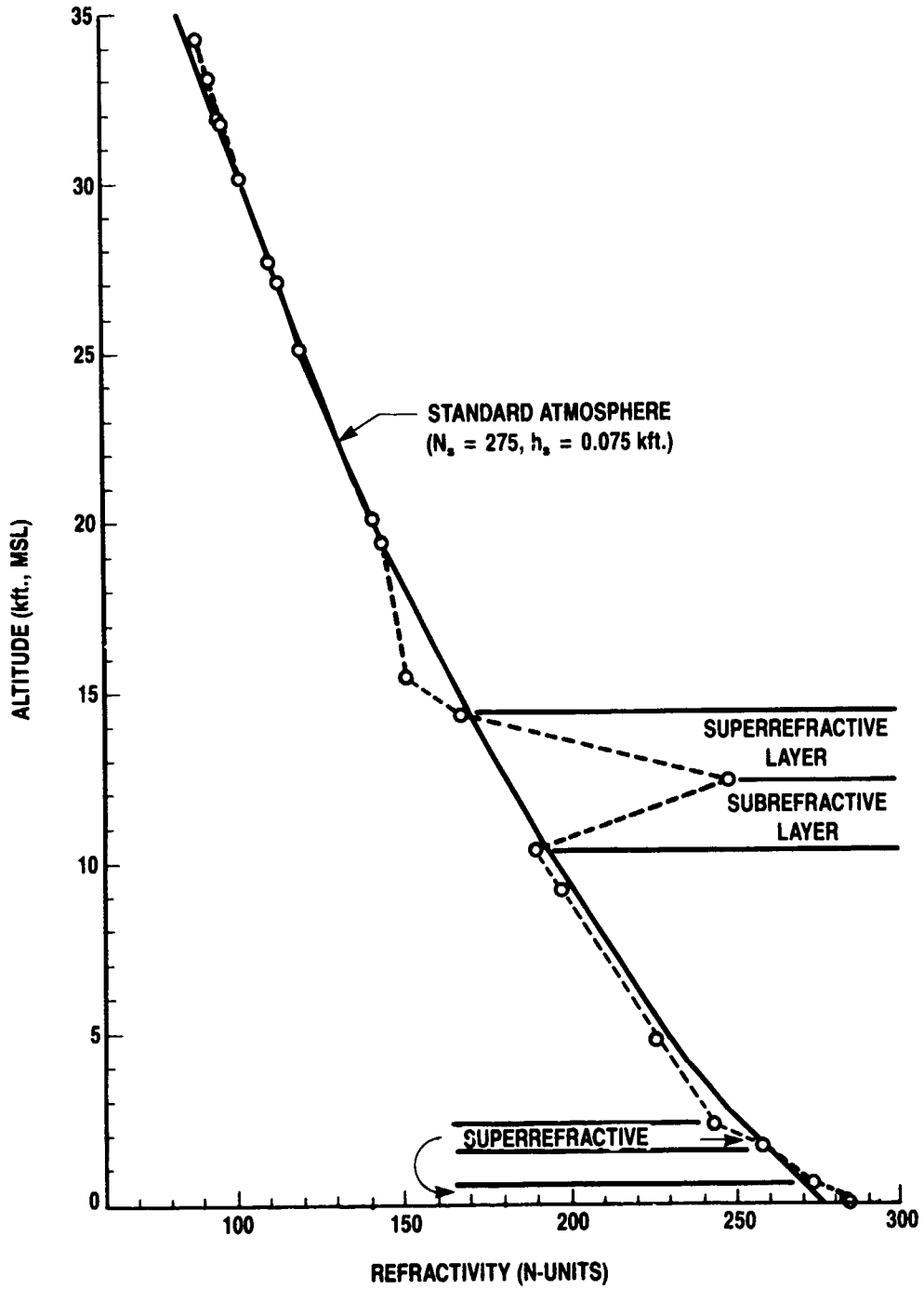

Figure 6. Measured and Standard Profile for Dhahran, June 5, 1978, 12:00 GMT

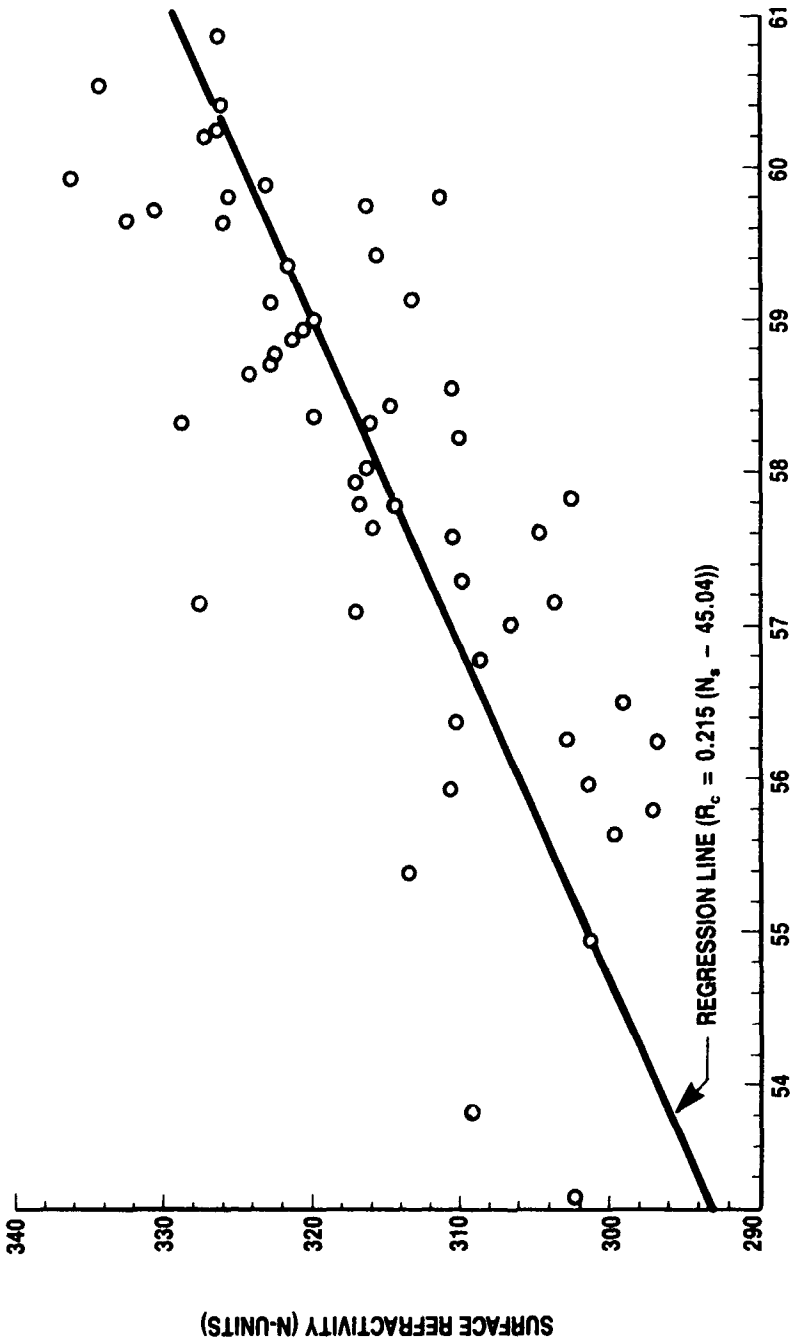

Figure 7. Surface Refractivity Versus Range Correction for Munich in August, 1978, 1980 - 12:00 GMT

The coefficient of correlation is 0.7772 -- a moderately high but still unimpressive value.

In figure 8, surface refractivity is plotted against range correction for 46 profiles obtained during June of 1978 and 1980 at Hannover, 0:00 GMT. Qualitatively, the scatter seen for this case is very similar to that observed in figure 7. The regression line is also comparable, and is given by:

$$R_C = 0.213\ [N_S - 54.13]$$

The coefficient of correlation is 0.7663.

Analysis analogous to the above has been performed for June of 1979 and 1980 at Dhahran (12:00 GMT) and for June of 1979, 1980, and 1981 at Pohang (0:00 GMT). In both cases, the scatter seen in plots like those of figures 7 and 8 was significantly greater, as corroborated by calculated correlation coefficients of about 0.55 for these cases. For the case of the Dhahran profiles, an additional stage of analysis was employed. Of the 56 profiles included in the original sample, 37, which contained abnormal* refractive gradients, were rejected. The remaining 19 profiles and corresponding range corrections were then treated separately, as shown in figure 9. Surprisingly, even for these "normal" profiles, scatter about the least squares fitted regression line is considerable, and qualitatively similar to that seen for the German (complete) sample sets of figures 7 and 8.

Although the correlation of range error and surface refractivity is not strong for the German sites, and even weaker for Dhahran and Pohang, the use of the surface refractivity for range correction estimation does appear to have some utility, especially if the data are available for the area of interest. To check for a relationship between mean range correction and mean surface refractivity, the appropriate data obtained from table 7 were used to produce the plots which appear in figure 10. If the Saudi Arabian data points are excluded because of the unusual atmospheric conditions often encountered there, the remaining three points for Munich, Hannover, and Pohang respectively, fall nearly on a straight line for each of the propagation geometries. The results of the linear regression

*Profiles were deemed abnormal if any atmospheric layer has an average refractivity gradient which is positive (subrefractive) or less than -7.88 N-units per 100 m (superrefractive).

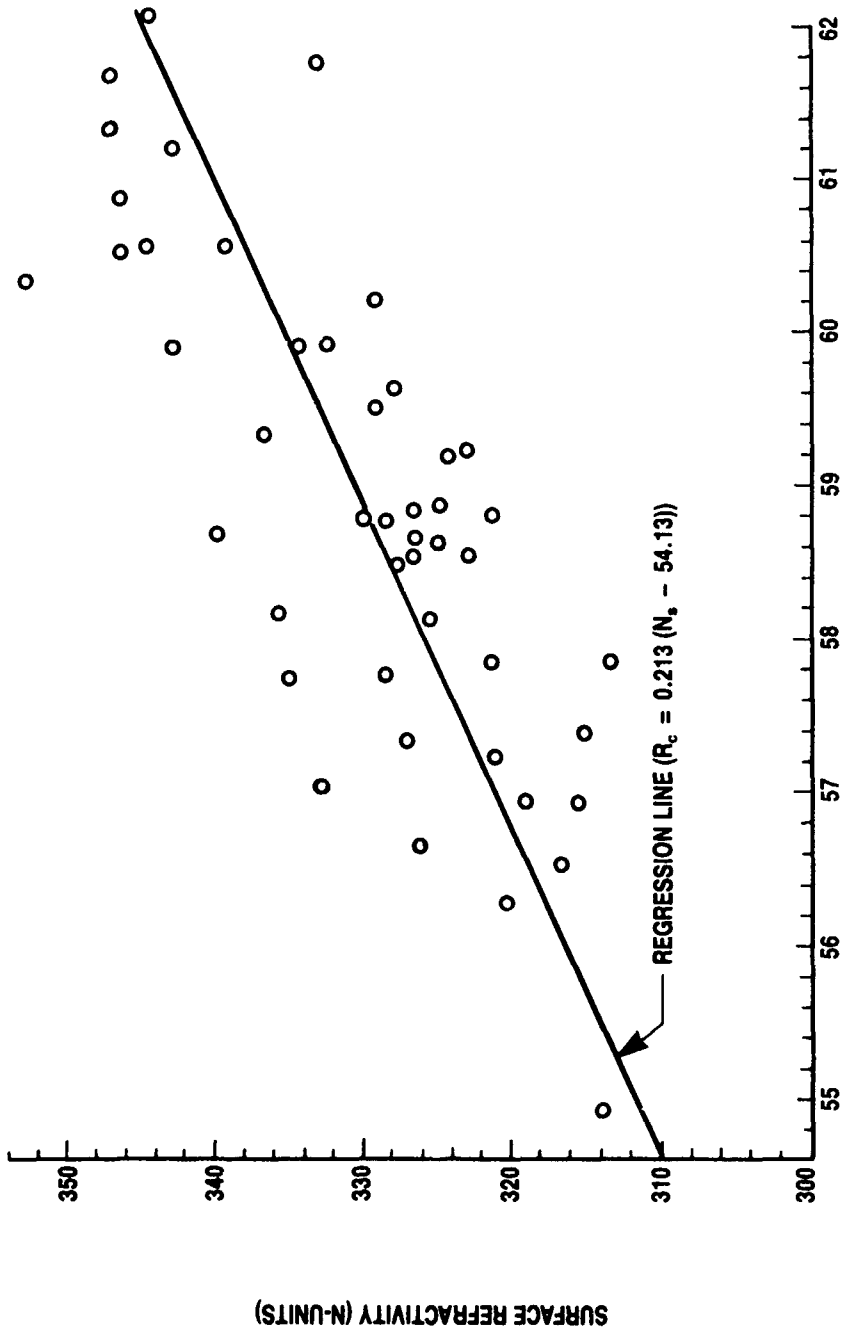

Figure 8. Surface Refractivity Versus Range Correction for Hannover in June 1978, 1980 - 0:00 GMT

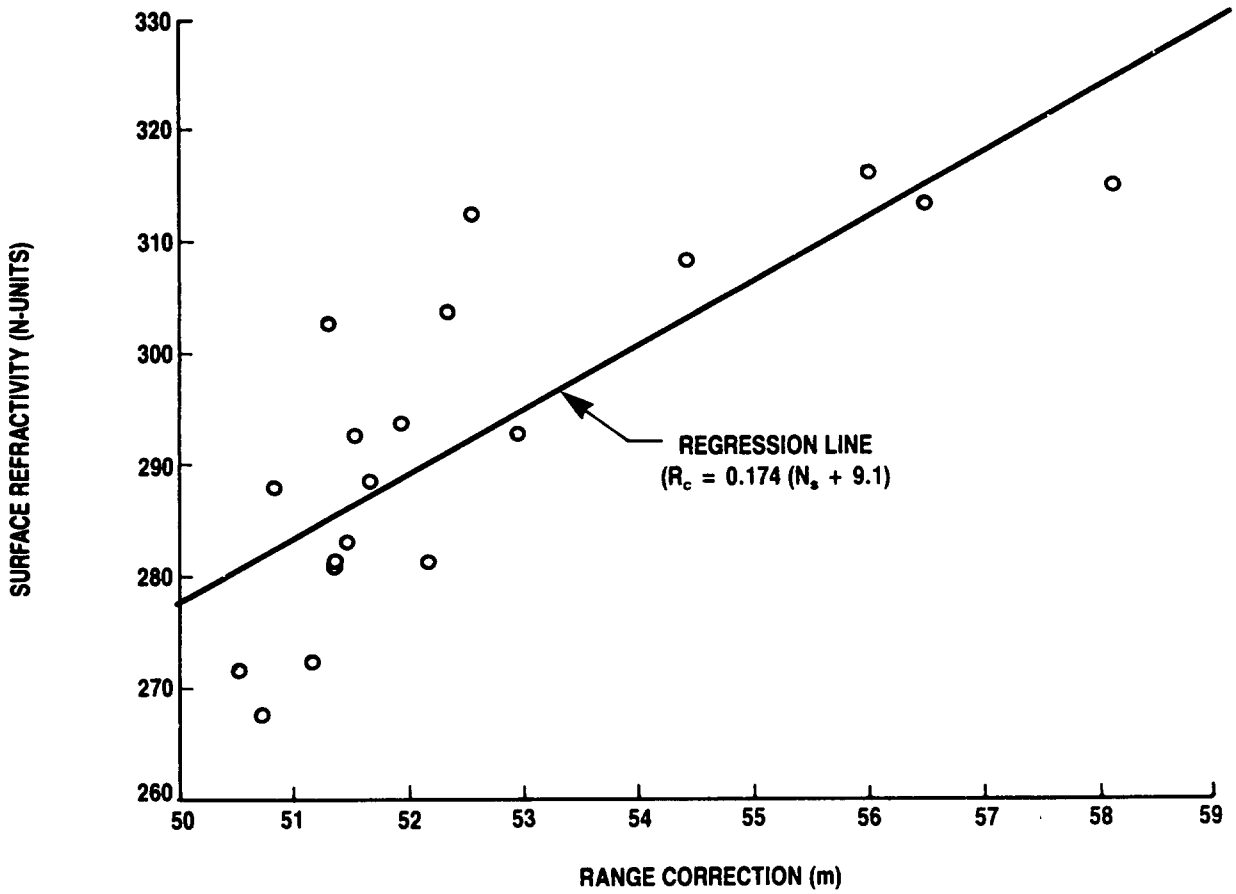

Figure 9. Surface Refractivity Versus Range Correction for Dhahran in June 1979, 1978 - 12:00 GMT

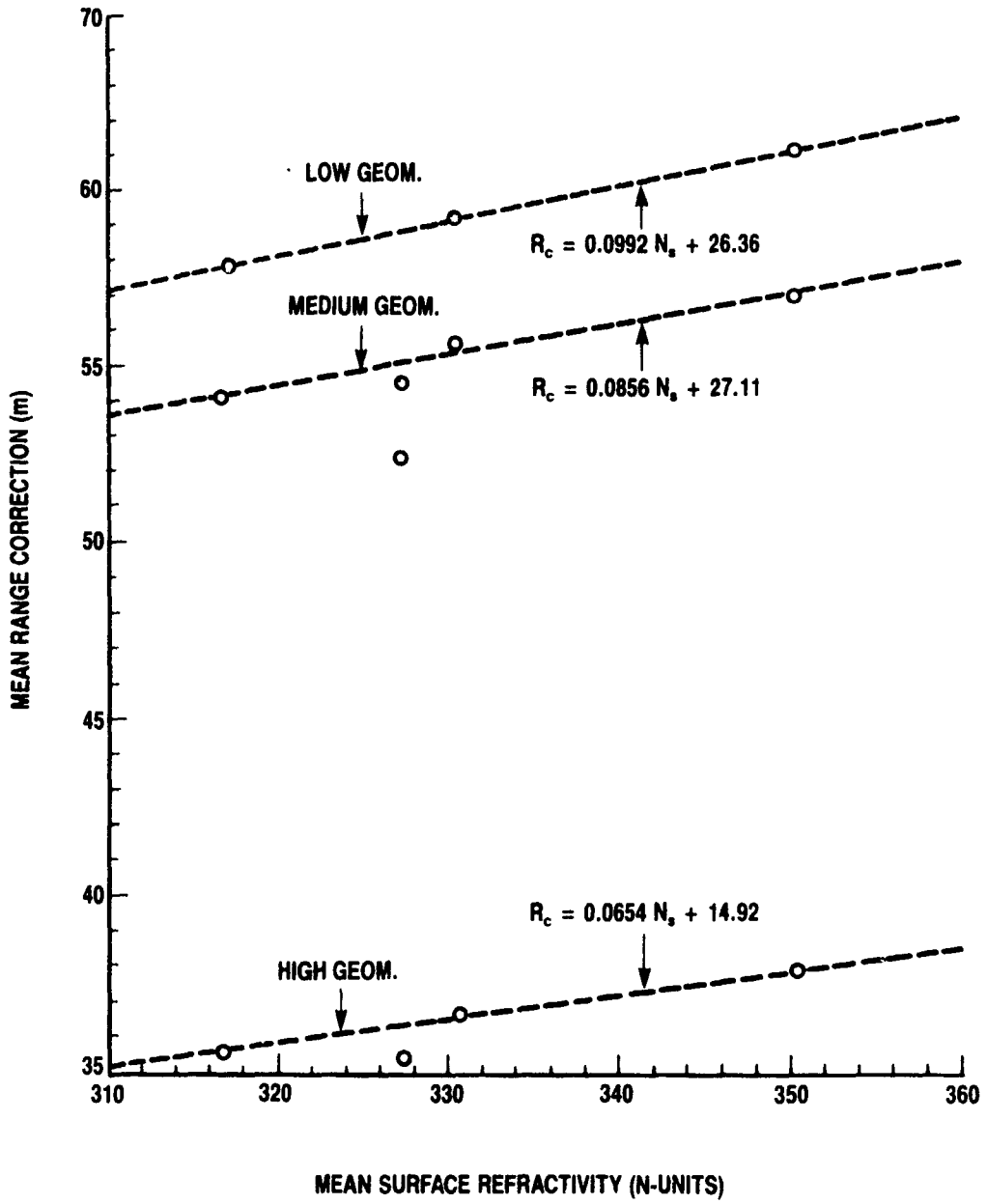

Figure 10. Mean Range Correction Versus Mean Surface Refractivity

analysis appear in table 9. Thus, with a notable exception, mean range correction correlates well with mean surface refractivity for the limited sample of sites presently available. As noted previously, the frequency of occurrence of strong superrefractive surface layers at Dhahran accounts for the abnormally high mean surface refractivity.

The principal conclusions of this section are: 1) the standard profile ray trace model can be used to provide more than adequate estimates for the mean radar range correction, and 2) the range correction variation with month, day, or time of day is small relative to the mean range correction and certainly small in comparison to Joint STARS accuracy requirements. A general empirical function for the range correction, based upon the standard atmosphere model, is presented in the following section.

Table 9

Linear Regression for Mean Range Correction
Versus Mean Surface Refractivity

Geometry	Correlation Coefficient	Regression Line
Low	0.9997	$R_C = 0.0992\ N_S + 26.4$
Medium	0.9861	$R_C = 0.0856\ N_S + 27.1$
High	0.9980	$R_C = 0.0654\ N_S + 14.9$

SECTION 6

STANDARD RANGE CORRECTION

The comparison of ETAC and MITRE ray trace results, which was presented and discussed in the previous section, indicates that the MITRE ray traces, which are based on a standard refractivity model[2], can be used to provide good estimates for mean range correction. Furthermore, the ETAC work shows that range correction variability is relatively small, as manifested by typical variation coefficients* of ~2%. The standard model can therefore be used with confidence to predict the mean range correction with reasonable accuracy.

Table 10 provides range correction values as determined for specific combinations of surface refractivity (N_s), radar altitude (h), and radar indicated range (R_t), in the context of the standard refractivity model and a terrain elevation of 1,000 ft. The parameters span a useful range of conditions and geometries which may be encountered by airborne radar. A general but simple analytical expression for the range correction would eliminate the need for interpolation and/or a lookup table. As indicated by equation (18), range correction is a function of N_s, h, and R_t. Close examination of table 10 reveals the following approximate relationships:

1. For a given surface refractivity and radar altitude, range correction is directly proportional to radar range (recall results of section 4).

2. For a given surface refractivity and radar range, the range correction is inversely proportional to the square root of the radar altitude.

3. For a given radar altitude and radar range, the range correction is directly proportional to the square root of the surface refractivity.

Taken together, these observations may be expressed:

$$R_c \propto R_t \left(\frac{N_s}{h}\right)^{\frac{1}{2}} \qquad (21)$$

*Variation coefficient = (Standard Deviation/Mean) x 100%.

Table 10

Range Corrections for Standard Model Atmosphere Ray Traces

SURFACE REFRACTIVITY (N-UNITS)	RADAR ALTITUDE (kft.)	RANGE CORRECTION (m) vs. RADAR RANGE (km)				
		40 km	80 km	120 km	160 km	200 km
250	15	8.0	16.1	24.4	33.0	42.1
	35	6.1	12.4	18.7	25.3	32.2
	45	5.4	10.8	16.3	22.1	28.2
	65	4.1	8.3	12.6	17.1	21.8
300	15	9.3	18.7	28.4	38.4	49.1
	35	6.8	13.7	20.7	28.1	35.9
	45	5.8	11.8	17.9	24.3	31.0
	65	4.5	9.0	13.7	18.5	23.7
350	15	10.4	21.1	32.0	43.4	55.6
	35	7.4	14.9	22.6	30.6	39.2
	45	6.3	12.7	19.3	26.2	33.5
	65	4.8	9.6	14.6	19.9	25.4
400	15	11.5	23.2	35.3	48.0	61.5
	35	7.9	15.9	24.2	32.9	42.1
	45	6.7	13.5	20.6	27.9	35.8
	65	5.1	10.2	15.5	21.0	26.9

To determine the constant of proportionality, a least mean squares linear regression fit of range correction versus the right side of (21) was performed for the 80 values of table 10. By this method, a general expression for the range correction,

$$R_c \cong A + B R_t \left(\frac{N_s}{h}\right)^{\frac{1}{2}} \tag{22}$$

$$A = 0.42 \text{ m}; \qquad B = 0.0577 \frac{\text{m}}{\text{km}} \left(\frac{\text{kft}}{\text{N-unit}}\right)^{\frac{1}{2}}$$

was deduced (coefficient of correlation = 0.9937). In the above, radar range has units of kilometers, radar altitude has units of kilofeet, and refractivity is in N-units. To check the fit produced by equation (22), table 11, which presents the predictions of equation (22) in the format of table 10, is provided. Under most circumstances, the estimate provided by equation (22) is within ±1 m of the standard model result. Although more sophisticated curve fitting methods would undoubtedly yield better correlation with the ray trace results of table 10, equation (22) has the advantage of great simplicity with a tolerable loss of accuracy.

In actual practice, measured surface refractivity at the surveillance site might be used in equation (22), or, if this information is not available, a seasonally adjusted average value would be employed. As discussed in section 5, a strong day by day correlation between surface refractivity and range correction is not apparent. However, the mean range correction can be accurately predicted by equation (22) if the mean surface refractivity ($\overline{N_s}$) is used. As seen, for example, in figure 10, Dhahran is an exceptional case, for which some downward adjustment of $\overline{N_s}$, to compensate for superrefractive surface layers, may be required.

Table 11

Range Corrections from Empirical Formula

SURFACE REFRACTIVITY (N-UNITS)	RADAR ALTITUDE (kft.)	RANGE CORRECTION (m) vs. RADAR RANGE (km)				
		40 km	80 km	120 km	160 km	200 km
250	15	9.0	18.4	27.8	37.3	46.7
	35	5.7	11.9	18.1	24.3	30.4
	45	5.0	10.5	15.9	21.3	26.8
	65	4.1	8.6	13.2	17.7	22.2
300	15	9.9	20.2	30.5	40.9	51.2
	35	6.3	13.1	19.9	26.6	33.4
	45	5.5	11.5	17.5	23.4	29.4
	65	4.5	9.5	14.5	19.4	24.4
350	15	10.7	21.9	33.0	44.2	55.3
	35	6.9	14.2	21.5	28.8	36.1
	45	6.0	12.5	18.9	25.3	31.8
	65	4.9	10.3	15.6	21.0	26.4
400	15	11.5	23.4	35.3	47.3	59.2
	35	7.4	15.2	23.0	30.8	38.6
	45	6.5	13.3	20.2	27.1	34.0
	65	5.3	11.0	16.8	22.5	28.2

SECTION 7

CONCLUSIONS

To provide an accurate estimate of the true range of a target, a long range airborne surveillance radar must account for refractive effects of the atmospheric medium, as described in section 3. The principal contribution to the range correction arises from the retardation of the electromagnetic waves, which is proportional to refractivity. It is therefore conceivable that unknown or uncontrollable atmospheric perturbations or anomalies, which affect the refractivity, may compromise the targeting accuracy of a modern radar. The present study, based largely on the USAFETAC ray trace work, finds that range correction, in the context of the Joint STARS propagation environment, can be implemented with sufficient accuracy to insure that system performance is not appreciably impaired by refraction effects.

A simple formula, such as equation (22) in the text, will provide adequate range correction for Joint STARS. Detailed atmospheric measurements at the surveillance site are not necessary and are usually impractical. Atmospheric variability introduces range correction variations with standard deviations of from 1-3 m. Prediction of the mean range correction for a given location would benefit from a knowledge of mean surface refractivity, as illustrated in figure 10. Measured mean surface refractivity might be adjusted in some cases, e.g., Persian Gulf sites, in order to compensate for known climatic and/or geographical peculiarities.

LIST OF REFERENCES

1. G. A. Robertshaw, "Effective Earth Radius for Refraction of Radio Waves at Altitudes Above 1 km," ESD-TR-83-219, Electronic Systems Division, AFSC, Hanscom AFB, MA (December 1983), A137095.

2. B. R. Bean, and G. D. Thayer, "Models of the Atmospheric Radio Refractive Index," Proceedings of the IRE, Vol. 47, May 1959, p. 744 (Also see op. cit. 1, Appendix A).

3. B. R. Bean et al., A World Atlas of Atmospheric Radio Refractivity, ESSA Monograph 1 (U.S. Government Printing Office, Washington, 1966).

APPENDIX A

RANGE CORRECTION HISTOGRAMS

The ETAC range correction values derived from the atmospheric profiles obtained at Munich, Hannover, Dhahran, and Pohang are displayed histographically in figures A-1 through A-4, respectively. The results are also broken down by month in order to show monthly variations.

The height of a bar or frequency denotes the number of cases (profiles) which produced range corrections bounded by the horizontal limits of that bar, i.e., range corrections which have values less than the right boundary and greater than or equal to the left boundary. For example, in figure A-1, a total of 52 cases have range corrections which satisfy,

$$57.0 \leq R_c < 57.5$$

and in figure A-3, a total of 59 cases have range corrections which satisfy,

$$53.0 \leq R_c < 54.0$$

For the two German sites, the monthly histograms are similar in both position and spread, apart from a small minority of cases which lie at the extremes. This observation is corroborated by the range correction statistics of tables 3 and 4, which vary little from month to month for each site. On the other hand, the monthly histograms which represent the range correction distributions for the Dhahran and Pohang sites exhibit relative position shifts of 2-4 meters. Once again, these observations are consistent with the range correction statistics which appear in tables 5 and 6. The noted correspondence is, of course, expected, since the mean range correction is a measure of the histogram's "center of gravity," and standard deviation is a measure of its spread or width.

More data would be required to determine, with good confidence, whether the small monthly variations observed for Dhahran and Pohang range corrections reflect seasonal variations or are simply a result of random factors.

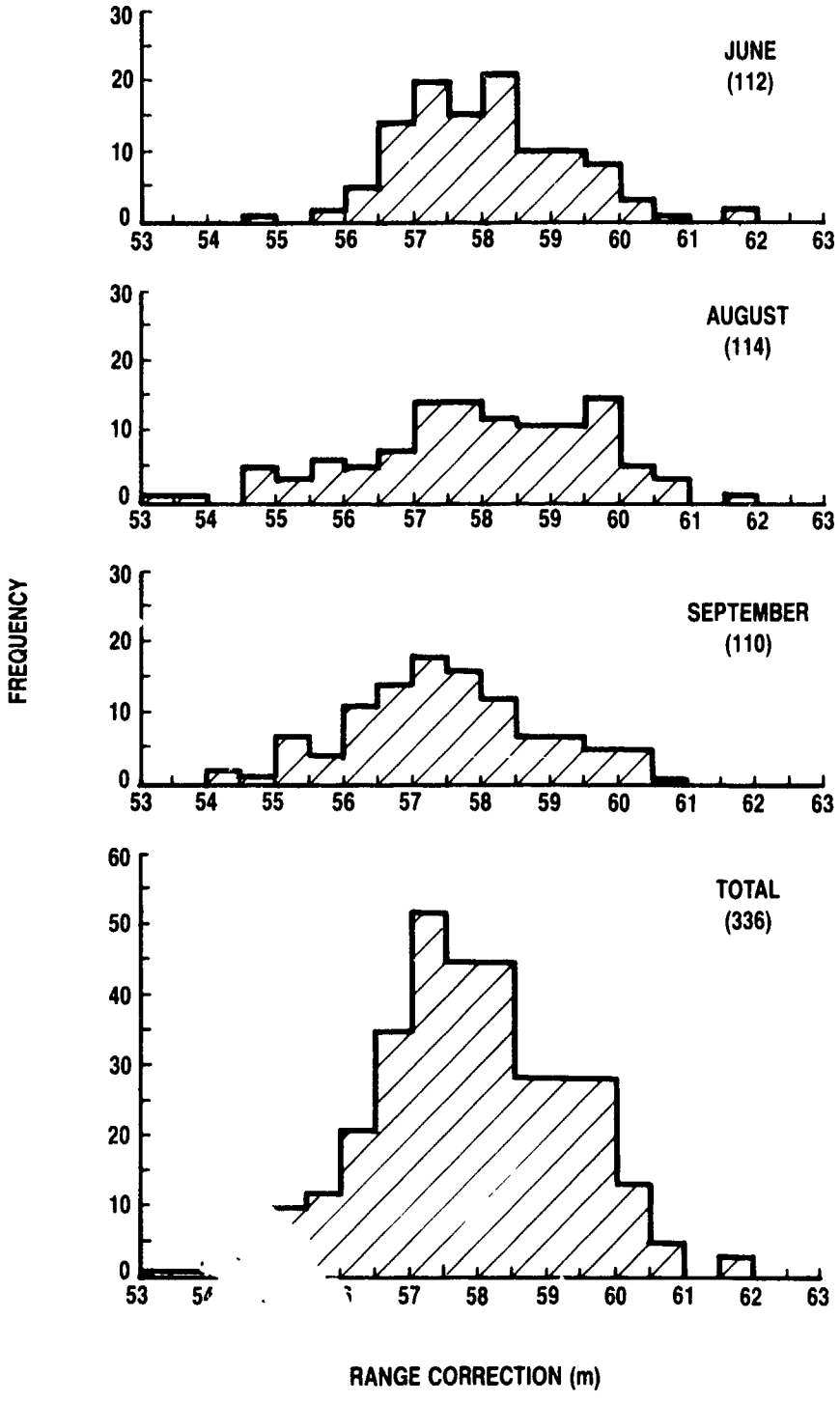

Figure A-1. Histograms for Munich Low Geometry Range Corrections

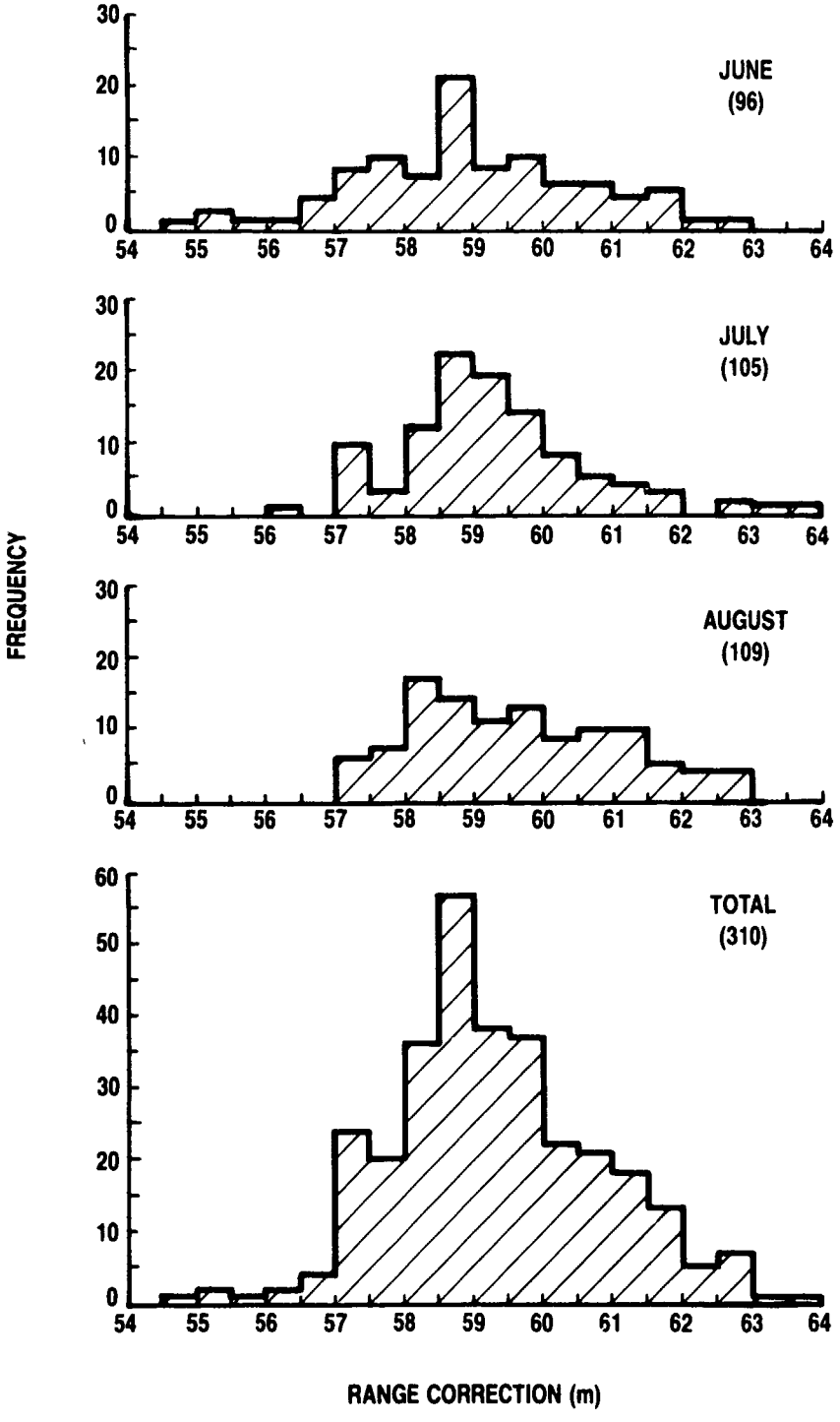

Figure A-2. Histograms for Hannover Low Geometry Range Corrections

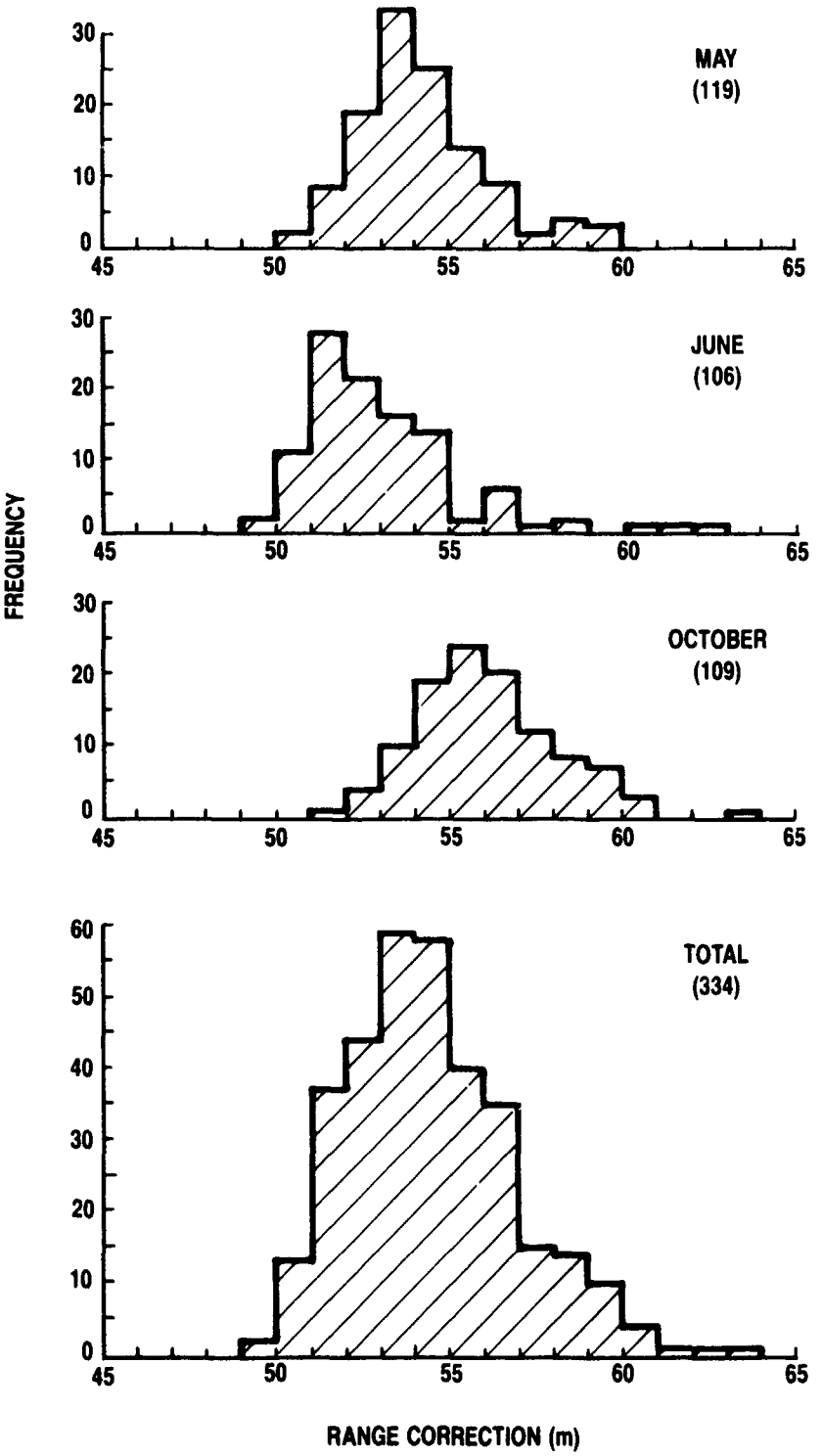

Figure A-3. Histograms for Dhahran Low Geometry Range Corrections

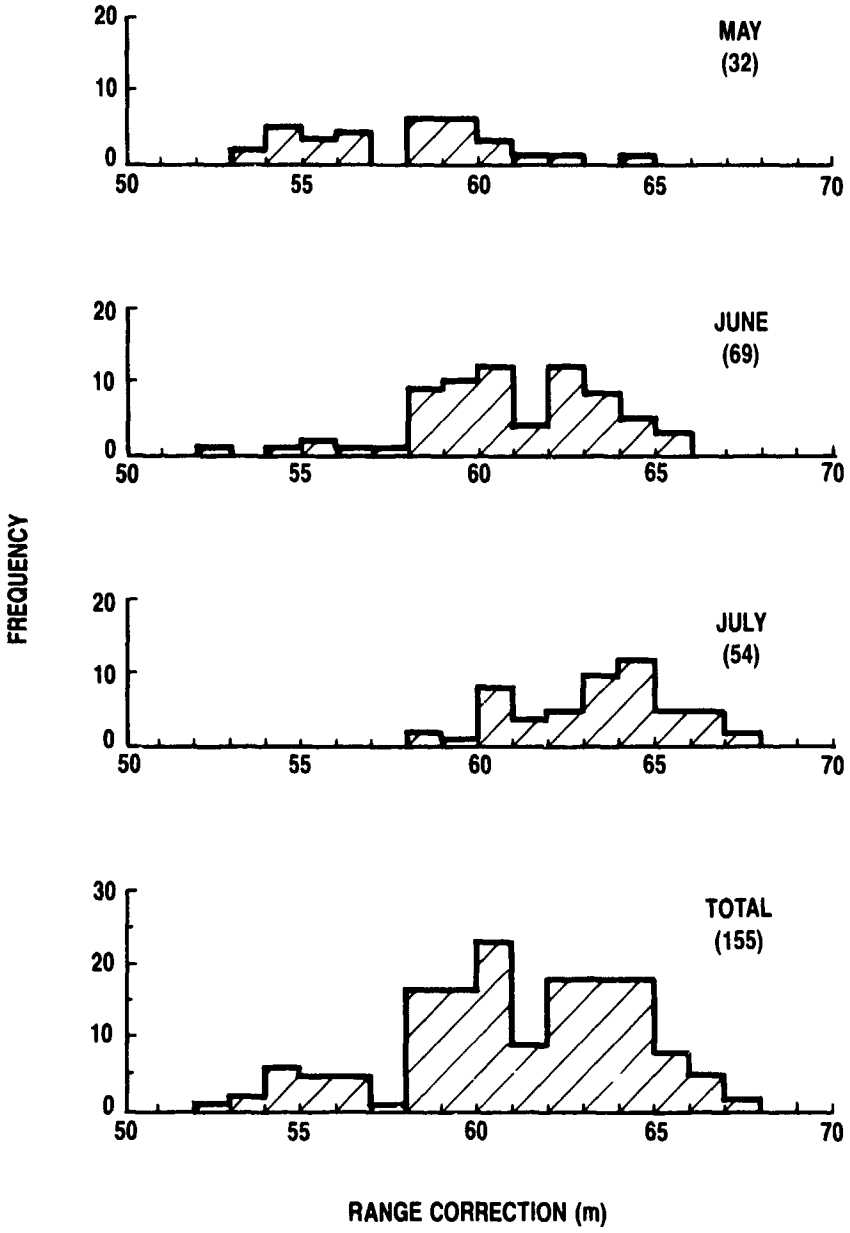

Figure A-4. Histograms for Pohang Low Geometry Range Corrections

APPENDIX B

CLIMACTIC BRIEFS FOR GERMANY, SAUDI ARABIA, AND KOREA

The following short climactic descriptions were excerpted from "Situation Climactic Briefs" USAFETAC (under Air Weather Service) at Scott AFB, IL. The discussion of anomalous propagation for the Arabian Peninsula was taken from "Propagation Climatology", Air Weather Service Forecaster Memo, FM-100/014.

Germany -- June through August

The summer is relatively cool and wet with frequent thunderstorms. Although there are occasional periods of hot, dry weather, cool and moist air from the North Atlantic Ocean normally blankets the area. Clear skies occur on 6-12 days per month during the summer. Visibility reaches a maximum at this time.

North Korea -- April and May

This is a period of transition between winter's dry northeast monsoon and summer's cloudy, wet, southwest monsoon. The southern regions are the cloudiest and wettest. Precipitation occurs on an average of 4-12 days per month with mean amounts ranging from 1 to 6 inches. Mean maximum temperatures range from the 50's (F) in the north to the 70's in the south. Mean minimum temperatures are near 30F in the north and in the low 50's in the south. Visibility is generally good, except for morning fog in the valleys, sea fog along the western coast, and smoke/haze near industrial centers. Surface winds are generally light, but gale force winds occasionally occur over higher terrain.

North Korea -- June through August

The southwest monsoon dominates the weather in Korea with widespread cloudiness, locally heavy precipitation, and warm to hot temperatures. Mean cloudiness is 60-85 percent. Mean rainfall ranges from 20 inches at southern locations in July to 3-6 inches at northeastern regions in August. Precipitation occurs on 10-20 days per month; thunderstorms occur on 3-9 days per month. Mean daily maximum temperatures are in the 80's (F) in the south and the 70's at northeast coastal regions. Mean minimum temperatures range from the 60's to 70's in the south to the 40's and 50's in the north. Visibility is fair to good except where morning valley fog, sea fog advected over western regions, and smoke/haze near industrial centers occur.

Surface winds are generally light, however, gale force winds occur on occasion at exposed locations in mountainous terrain. Weakening typhoons and tropical storms affect the western and southern coast producing high winds and torrential rains.

Saudi Arabia -- April through October

The summer season is frequently cloudless, hot, and dry. Mean cloudiness ranges from about 3 percent in the desert interior to approximately 10 percent along the Red Sea and Arabian Gulf coast. Daily minimum temperatures are in the 60's to 80's (F). Daily maximum temperatures are in the 90's to 110's. Rainfall is rare. Mornings are characterized by calm winds while afternoons are characterized by desert winds which usually reach 17 knots or greater. Gale force winds may occur in the desert interior. The strong afternoon winds cause frequent sandstorms/dust storms. Heat shimmer during the day may severely limit horizontal visibility.

Propagation Climatology for the Arabian Peninsula

The Arabian Peninsula consists largely of arid plains that are bordered by hills and mountains in the northeast, southwest, and to some extent the southeast. Climate controls are from the semi-permanent pressure systems, winter time migratory systems, and topography. The Arabian Peninsula summers are hot, dry, and almost cloudless. The winters are mild with only moderate cloudiness in the northern regions. A more complete description of the climate/weather regimes of the Arabian Peninsula, is contained in AWS/FM-100/009.

The anomalous propagation environment of this region is among the most severe in the world.* Subrefractive and superrefractive gradients in both surface and elevated layers are common throughout the year.

The geographical location of the Arabian Peninsula and its proximity to the modifying influence of the Persian Gulf, Gulf of Oman, Arabian Sea, Gulf of Aden, and Red Sea combine to produce a unique climatology with respect to tropospheric propagation. The interse heating of the nearly overhead sun produces superadiabatic lapse rates in the lower layers during the midday portion which may lead to the formation of subrefractive gradients which may persist for several hours. Although the greatest frequency of occurrence is during the summer months, situations such as these are common throughout the year.

*Emphasis added.

The rapid cooling of the layer of air adjacent to the surface produces superrefractive layers at night which often are intense enough to trap low elevation angle radiation propagated from surface based systems at VHF and above.* These layers normally dissipate after sunrise.

The greatest frequency of superrefractive/ducting gradients are observed during the summer months along the coastal sections of the peninsula. These coastal layers occur as a result of the combination of the contrast between the high sea surface temperature in the waters surrounding the peninsula coupled with the flow of extremely hot, dry air over the surrounding seas. This condition is enhanced by the presence of subsidence over the entire region throughout the year except for brief frontal activity during the winter months.

The high evaporation rates over the surrounding seas as a result of the high sea surface temperature coupled with the advection of the dry air out over the water also are conducive to the formation of fog which occasionally produces subrefractive gradients but most often contributes to the formation of intense advective ducts.

Heavy rainfall which can severely attenuate EM energy in the SHF-EHF range is usually not a problem. However, the westward extension of the southwest monsoon occasionally produces brief periods of heavy rainfall. This situation would be most likely to be expected along the Yemen and Oman coastlines.

The high absolute humidity in the lowest layer of the air along the coastal sections and over the surrounding water is the highest in the world. Absolute humidities of 25 g m^{-3} are common and occasionally 35 g m^{-3} can be observed. The high water vapor content may produce attenuation of up to 0.5 dB km^{-1} at certain frequencies.

*Emphasis added.